

# Pit chains on Enceladus signal the recent tectonic dissection of the ancient cratered terrains



Emily S. Martin<sup>a,b,\*</sup>, Simon A. Kattenhorn<sup>c</sup>, Geoffrey C. Collins<sup>d</sup>, Robert L. Michaud<sup>d</sup>, Robert T. Pappalardo<sup>e</sup>, Danielle Y. Wyrick<sup>f</sup>

<sup>a</sup> Department of Geological Sciences, University of Idaho, Moscow, ID, 83844, United States

<sup>b</sup> Center for Earth and Planetary Studies, National Air and Space Museum, Smithsonian Institution, Washington, D.C. 20560, United States

<sup>c</sup> Department of Geological Sciences, University of Alaska Anchorage, Anchorage, AK 99508, United States

<sup>d</sup> Physics and Astronomy Department, Wheaton College, Norton MA, 02766, United States

<sup>e</sup> Jet Propulsion Laboratory, California Institute of Technology, Pasadena, CA, 91109, United States

<sup>f</sup> Southwest Research Institute, San Antonio, TX, 78238, United States

## ARTICLE INFO

### Article history:

Received 28 October 2016

Revised 9 March 2017

Accepted 10 March 2017

Available online 12 March 2017

### Keywords:

Tectonics

Saturnian satellites

Enceladus

Fractures and faults

## ABSTRACT

Enceladus is the first outer solar system body on which pit chains have been positively identified. We map the global distribution of pit chains and show that pit chains are among the youngest tectonic features on Enceladus's surface, concentrated in the cratered plains centered on Enceladus's Saturnian and anti-Saturnian hemispheres. Pit chains on Enceladus are interpreted as the surface expressions of subsurface dilational fractures underlying a cover of unconsolidated material, which we infer to be a geologically young cover of loose regolith that mantles the surface of Enceladus. A widespread layer of regolith may act to insulate the surface, which has implications for the thermal state of Enceladus's ice shell. The widespread distribution of pit chains across the cratered plains indicates that this ancient surface has recently been tectonically active.

© 2017 Elsevier Inc. All rights reserved.

## 1. Introduction

Pit chains are collinear assemblages of circular to elliptical depressions (Fig. 1) that are widespread on solid-surface bodies across the solar system. These landforms have been described on Venus (Bleamaster et al., 2004), Earth (Okubo and Martel, 1998; Ferrill et al., 2004, 2011; Wyrick et al., 2004), Mars (Wyrick et al., 2004; Ferrill et al., 2004), and several small solar system bodies, including Phobos (Thomas et al., 1979; Hurford et al., 2016), Eros (Prockter et al., 2002; Buczkowski et al., 2008), Gaspra (Veverka et al., 1994), Ida (Sullivan et al., 1996), and Vesta (Buczkowski et al., 2012a,b,2013; Wyrick et al., 2010) (Fig. 1). Pit chains across the solar system form by a variety of mechanisms, including karst, lava tube collapse, venting processes, extensional fracturing, or dilational faulting (e.g., Wyrick et al., 2004, 2010). Pit chains have also been identified on Enceladus (Michaud et al., 2008); therefore, characterizing the mechanism by which pit chains form on

Enceladus will provide insights into the manner in which its icy shell deforms and will further unravel the complex and dynamic geologic history of this moon.

Enceladus's active plume (Porco et al., 2006) and thermal anomaly (Spencer et al., 2006) within the South Polar Terrain (SPT) make Enceladus one of the few geologically active bodies in the solar system and a primary astrobiological target. These SPT jets act as a source of fall-back material that may have mantled Enceladus's surface (Porco et al., 2006; Kempf et al., 2010) and, in part, contributed to the muted morphologies of craters (Bray et al., 2007; Kirchoff and Schenk, 2009; Bland et al., 2012) and tectonic landforms observed across Enceladus (Crow-Willard and Pappalardo, 2015). Therefore, any recent tectonic dissection of the surface would necessarily have interacted with this mantled surface. Pit chains were initially reported within the ancient cratered plains (Fig. 2) centered near the Saturnian (0°) and anti-Saturnian (180°) points (Michaud et al., 2008). Here, we aim to characterize pit chains on Enceladus and determine their likely formation mechanism(s) by assessing their spatial distribution, their age relative to other terrains, and their relationship or interaction with the recently mantled surface.

\* Corresponding author at : Center for Earth and Planetary Studies, National Air and Space Museum, Smithsonian Institution, Washington, D.C. 20560, United States. E-mail address: [martines@si.edu](mailto:martines@si.edu) (E.S. Martin).

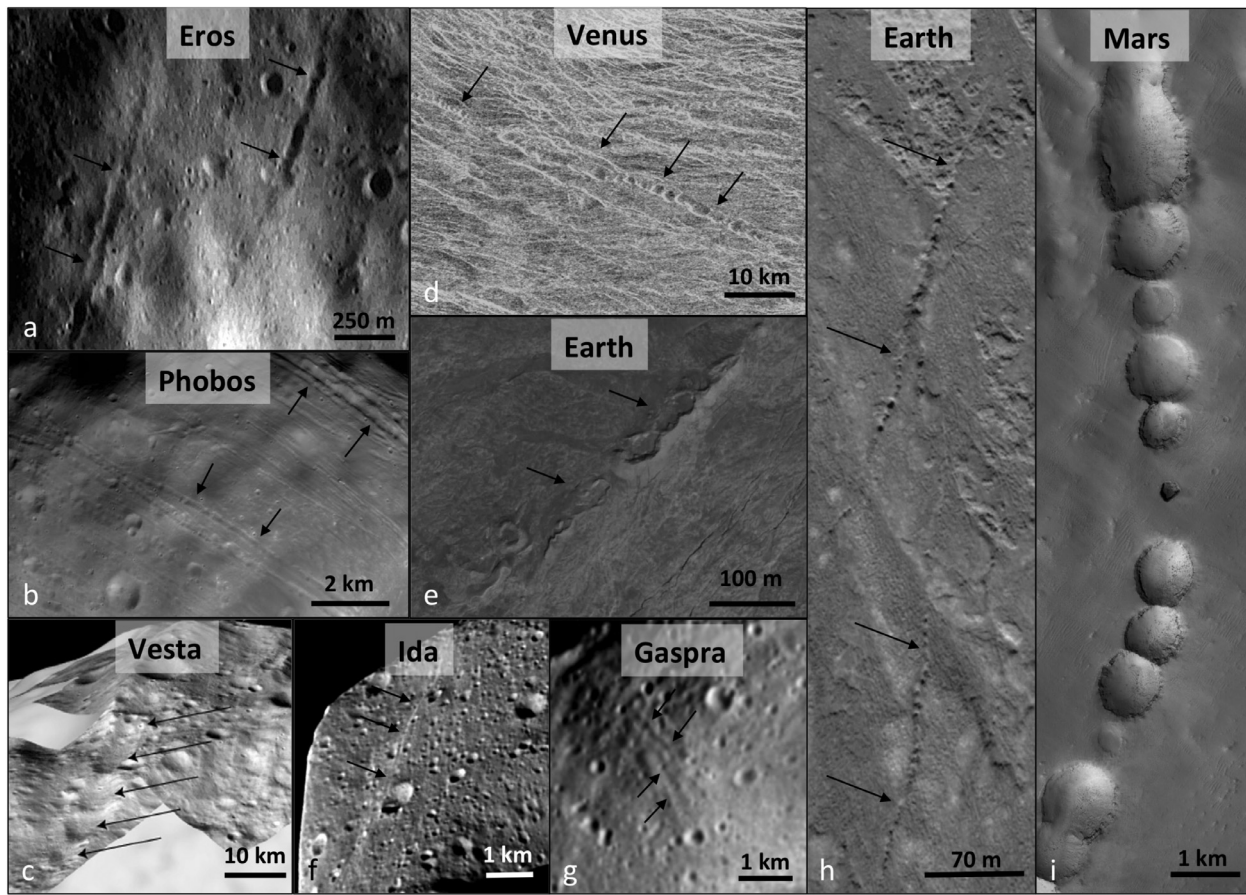


**Fig. 1.** The morphology of pit chains across the solar system. **a.** Eros from NEAR. Image no. 135344864 (Buczkowski et al., 2008). **b.** Phobos. Image PIA10367. **c.** Albalonga Catena, Vesta. Modified after Buczkowski et al. (2013). **d.** Venus. Right-look Magellan data near 13°S, 112°E (Bleamaster et al., 2004). **e.** Kilauea Volcano, Hawaii centered at 19.3909°N 155.3076°W. Image taken 12/06/2014, acquired from Google Earth on 04/20/2016. **f.** Ida, modified from image PIA00332. **g.** Gaspra, modified from Galileo image PIA00332. **h.** Pit chains in northeastern Iceland centered near 65.9902°N and 16.5301°W (see also Figs. 3a & 5 in Ferrill et al., 2011). Image taken on 7/27/2012, acquired from Google Earth 04/20/2016. **i.** Pit chains on Mars from the Mars Global Surveyor Mars Orbiter Camera, centered near 6.5398°S and 119.9703°W on the flank of Arsia Mons. Image PIA02874.

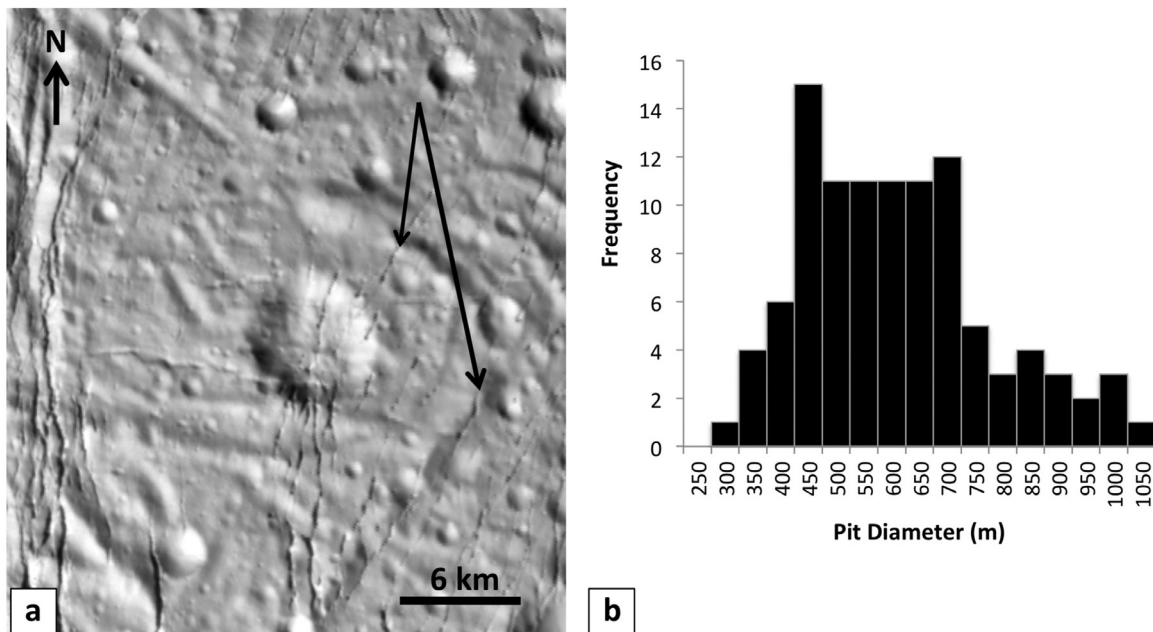


**Fig. 2.** **a.** Pit chains on Enceladus are composed of collinear, isolated pits. Cassini ISS Image No. N1489050144 centered at 4°E, 152°N with a resolution of 75 m/pixel. **b.** A histogram of pit chain diameters showing a range of 300–1000 m. The population represented in this histogram are from a sampling of pits across the surface.

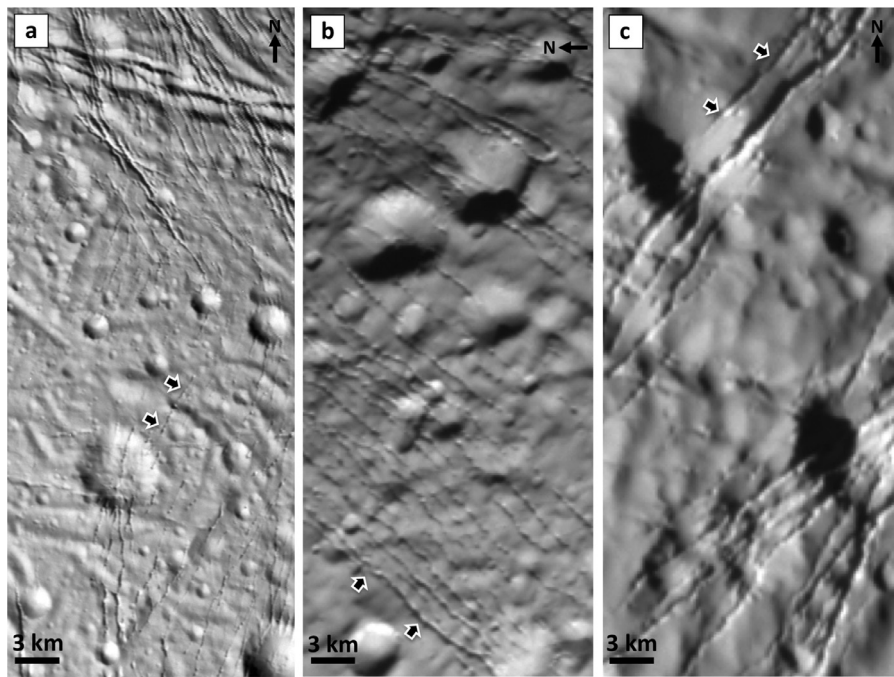


**Fig. 3.** Examples of different pit chain morphologies on Enceladus (Martin and Kattenhorn, 2013, 2014; Nahm and Kattenhorn, 2015). **a.** Chains of isolated pits. Image no. 1489050078 (77 m/pixel). **b.** Pit chains comprised of partially merged pits. Image no. N1500061010 (134 m/pixel). **c.** Fully merged pit chains characterized by scalloped edges along the trough rim. Image no. N1500061010 (134 m/pixel). Arrows highlight individual examples of each of the three morphologies.

## 2. Observations

High-resolution images (i.e., 40–200 m/pixel) from the Cassini Imaging Science Subsystem (ISS) camera were used to produce a detailed, global-scale map of the distribution of pit chains across Enceladus. Raw images from the Planetary Data System (PDS) were processed using the USGS Integrated Software for Images and Spectrometers (ISIS). Individual high-resolution images were superimposed on a global mosaic of Enceladus (Roatsch et al., 2013) and pit chains were mapped in an ArcGIS environment.

### 2.1. Pit chain morphology and morphometry

Pit chains on Enceladus occur as aligned sets of circular and elliptical depressions (Fig. 2) that lack elevated rims or impact ejecta, and do not appear to modify the surface beyond their edges. Pit diameters measured perpendicular to the strike of the chain and were observed to be 300–1000 m in diameter, with the bulk of pit diameters at 450–700 m (Fig. 2b). The spacing between individual pits within a single chain is ~200–500 m. Pit chains occur as parallel sets with the spacing between pit chains within a set range from 500–2000 m. The morphology of pit chains on Enceladus is variable (Fig. 3) (Martin and Kattenhorn, 2013, 2014; Nahm and Kattenhorn, 2015) and all pit chain morphologies may exist within a given pit chain set (Wyrick et al., 2004; Nahm and Kattenhorn, 2015). Some pit chains appear as shallow, muted linear depressions along which occur isolated pits (Fig. 3a). Other pit chains consist of evenly spaced pits, commonly with adjacent pits within a single chain touching or even merging (Fig. 3b). Others, still, appear as scalloped to irregular linear depressions, where individual pits appear to have fully merged along a lineament or trough, creating the appearance of a continuous dilational crack (Fig. 3c). We identify troughs or sets of troughs with irregular rims as pit chains on the basis of their spatial association other pit chains.

### 2.2. Global distribution of pit chains

Global mapping of pit chains (Fig. 4) supports the predominance of pit chains within the cratered plains noted by Michaud et al. (2008), from 60°S to 55°N. We additionally observe a group of pit chains in the tectonized terrains on the trailing hemisphere centered at 60°E; these pit chains have no distinct morphological difference from those observed elsewhere on Enceladus. The large-scale topographic basins observed from stereogrammetry across 50% of Enceladus (Schenk and McKinnon, 2009) share no spatial relationship to the distribution of Enceladus's pit chains. Pit chains have not been observed above 55°N; although this paucity of pit chains within the north polar terrains may be an observational bias due to low-resolution coverage. It is also possible that whatever mechanism forms pit chains on Enceladus is not occurring or pit chains have not been preserved in these northern regions.

Pit chains within the cratered terrains form in groups of evenly spaced, regionally parallel sets (Fig. 3). These sets have similar geometric patterns and evidence of mechanical interactions in fracture growth paths to those observed in terrestrial joint sets (e.g., Cruikshank and Aydin, 1995).

### 2.3. Relative ages of pit chains

Pit chains are observed predominantly crosscutting the cratered plains (Fig. 4), which are interpreted as ancient (~4 Ga) terrains based on the high areal density of impact craters (Kirchoff and Schenk, 2009). However, pit chains also crosscut other terrains (Fig. 5), superposing many regions interpreted to be relatively geologically young. For example, Enceladus's tectonized terrains have been inferred as relatively young based on global geologic mapping (Crow-Willard and Pappalardo, 2015), and the trailing hemisphere tectonized terrains have been dated using crater densities to 0.02–2 Ga (Kirchoff and Schenk, 2009) (Fig. 5a, b). The superposition of pit chains within parts of the tectonized terrains suggest that at least some pit chains formed more recently than the process(es) that rendered these tectonized terrains. Pit chains are also found

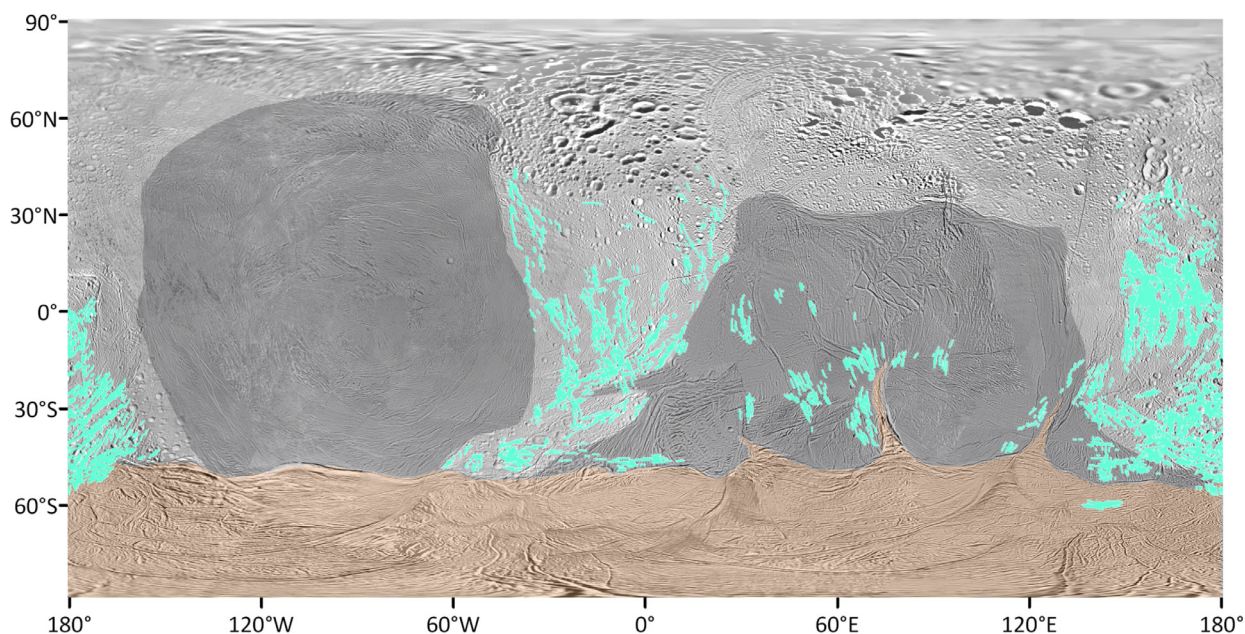


**Fig. 4.** Global distribution of pit chains. Shaded grey regions are the tectonized terrains; tan regions are the southern curvilinear terrains (Crow-Willard and Pappalardo, 2015) and South Polar Terrains. The remaining regions are cratered terrains. Pit chains are concentrated within the cratered terrains (centered near 0° and 180°), but some are observed within the trailing hemisphere tectonized terrain (near 60°E). Basemap credit: NASA/JPL-Caltech/SSI; Roatsch et al. (2013).

at the boundaries between the cratered terrains and the tectonized terrains (Fig. 5e, f), commonly in en echelon patterns, suggestive of relatively young shear motion at terrain boundaries (Martin, 2016). The low occurrence of craters in the southern curvilinear terrains and proximity to the geologically active SPT implies a relatively young age for these terrains (Crow-Willard and Pappalardo, 2015). Nonetheless, the southern curvilinear terrains are also crosscut by pit chains (Fig. 5c, d), implying that at least some stages of pit chain formation are geologically recent.

### 3. Discussion

#### 3.1. Pit chain formation mechanisms

Pit chains on rocky bodies may form through a variety of mechanisms (Fig. 6); therefore, we briefly discuss here the likelihood of each of these mechanisms in the context of Enceladus and the implications of the favored mechanisms on pit chain evolution and the impact of plume activity.

##### 3.1.1. Secondary impact craters

Secondary impact craters typically occur in clusters or chains (Fig. 6a) that radiate from a central point. Secondaries also have morphological characteristics in common with primary impact craters, such as raised rims and ejecta. Additionally, secondary impact structures may be associated with a diagnostic herringbone pattern (Fig. 6a), have non-circular rims, and low depth-to-diameter ratios (e.g., Oberbeck and Morrison, 1974; Pike and Wilhelm, 1978; McEwen and Bierhaus, 2006). There is no evidence for either the V-shaped herringbone ridges around any of the circular depressions in the pit chains, or for clustering of the depressions. Furthermore, pit chains on Enceladus lack elevated rims or ejecta, and occur in parallel (rather than radiating) sets, which is inconsistent with formation as secondary impact structures.

##### 3.1.2. Lava tubes

Lava tubes are subsurface channels created when low-viscosity lavas develop thick crusts above a channelized flow to form a roof.

Lava tubes form in the downslope direction and can have non-linear surface traces. The collapse of roof sections of lava tubes leads to aligned sets of pits, a process that has been observed on the Earth, the Moon (Haruyama et al., 2009), and Mars (Cushing et al., 2007) (Fig. 6b). Observed cryovolcanic activity on Enceladus is explosive rather than effusive and appears contained within the SPT (e.g., Porco et al., 2006; Spencer et al., 2009). Additionally, pit chains on Enceladus appear to form independent of topography (cf. Schenk and McKinnon, 2009); lava tubes will follow pre-existing downslope topography. Moreover, no plausible flow fronts or source vents for effusive volcanic activity have been observed anywhere on Enceladus suggesting that perhaps Enceladus has never experienced any kind of effusive volcanism.

##### 3.1.3. Karst dissolution

Pit chains associated with karst dissolution form due to flow of a liquid solvent within a soluble material (Fig. 6d). Compositionally, the shell of Enceladus is dominated by water ice (Brown et al., 2006), and there is no plausible solvent that is stable in liquid form near the surface of Enceladus because of temperature and pressure conditions. In addition to posing a difficulty for ice shell dissolution, relying on water from an underlying ocean to thermally erode near-surface ice is problematic from an energy standpoint. The bulk of the ocean should be in thermal equilibrium with the base of the ice shell, which results in a lack of excess heat needed to erode subsurface channels. Furthermore, the density contrast of liquid water and water ice is incompatible with sustaining a fluid flowing sufficiently near the surface to cause collapse. The dearth of evidence supporting an active groundwater circulation cycle on Enceladus makes karst dissolution an unlikely scenario for pit chain formation.

##### 3.1.4. Venting

Venting, or explosive cryovolcanism due to heating and escape of subsurface volatiles, would leave behind a void that allows regolith drainage, plausibly forming pit chains. We define “regolith” as a layer of unconsolidated or disaggregated material that overlies the solid portion of the icy crust, independent of source or genesis. Venting-induced formation of pits may show accompanying

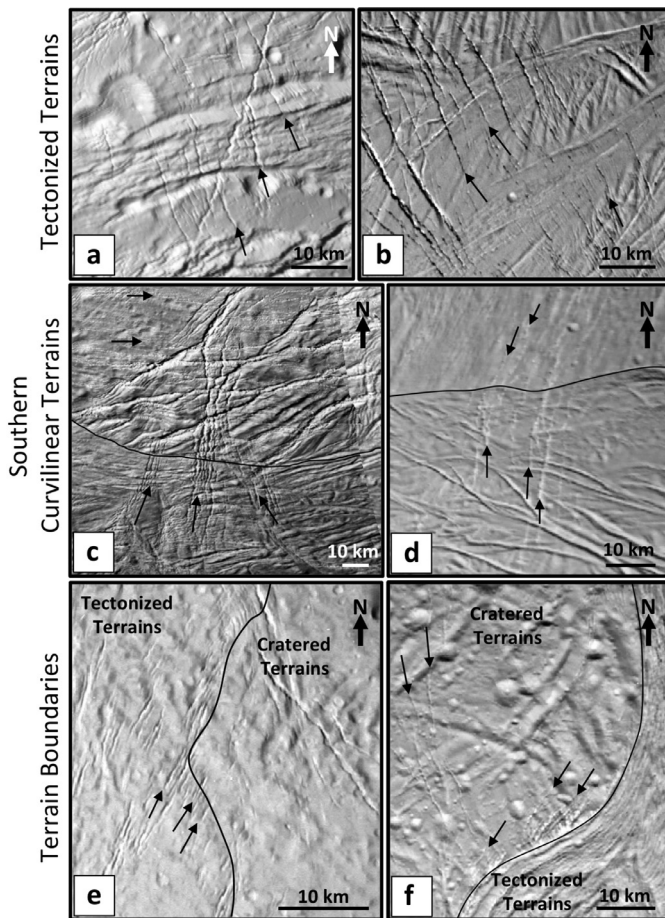


**Fig. 5.** Pit chains are among the youngest features on the surface of Enceladus. Examples of pit chains in each image are highlighted by black arrows. **a, b.** Pit chains crosscutting the tectonized terrains. **c, d.** Pit chains overprinting the geologically young southern curvilinear terrains encompassing the South Polar Terrain. The northern boundary of the southern curvilinear terrains is approximated by a black line. **e, f.** Pit chains at terrain boundaries, commonly in en echelon arrays. Terrain boundaries are approximated by black lines. Cassini image numbers: **a.** N1637465942, 137 m/pixel (centered at 4.933°W, 23.014°S); **b.** N1487300854, 118 m/pixel (centered at 50.709°E, 124.364°S); **c.** N1652859224, 204 m/pixel (centered at 32.228°W, 53.51°S); **d.** N1487300107, 148 m/pixel (centered at 92.09°E, 15.153°S); **e.** N1652863294, 264 m/pixel (centered at 35.939°W, 5.574°N); **f.** N1487300482, 132 m/pixel (centered at 24.143°E, 18.5°N).

evidence of volcanism such as flow features, cinder cones, fissure eruptions, or maar explosions (e.g. Okubo and Martel, 1998; Thorndarson and Larsen, 2007). Venting was proposed as the mechanism for a 3–6 km wide chain of pits radial to Ali Baba crater, as seen in *Voyager* data of Enceladus' northern hemisphere (Kargel, 1984). Cassini data revealed this feature in greater detail, showing no evidence for venting or a linear assemblage of pits and casting doubt on any resemblance to the pit chains described here. Nonetheless, Cassini data have led to the direct observation of venting along the jets emanating from the so-called tiger stripes: eruptive cracks near the south pole of Enceladus (Fig. 7) (Porco et al., 2014). Possible driving mechanisms for the venting include direct vaporization of subsurface ocean water (Spencer et al., 2006), shear heating (Nimmo et al., 2007), dissociation of clathrates (Kieffer et al., 2006), and fissure eruptions (Spitale et al., 2015; Kite and Rubin, 2016). The margins of the tiger stripes are elevated above their surroundings (~150–260 m (Patthoff et al., 2014)), are relatively straight (Spencer et al., 2009), and relatively wide (~2 km (Porco et al., 2006)). No nozzle-like individual vents, cones, or pitting from which particulate material may have explosively emanated have

been observed along the tiger stripes (Fig. 7). The pits within pit chains observed on Enceladus show no substantial topographic expressions and are of the order of 200–500 m in width. The lack of morphological similarity between the pit chains and the tiger stripes therefore casts doubt on venting as a likely mechanism for pit chain formation on Enceladus.

### 3.1.5. Extension fractures and dilational faulting

Pit chains can be produced by the opening of mode I tension fractures (i.e., joints) or along high-angle normal faults beneath a loose unconsolidated regolith (e.g., Ferrill et al., 2004; Wyrick et al., 2004). Both extension fracturing and dilational faulting result in subsurface voids into which loose material on the surface can drain, creating linear assemblages of pits (Ferrill et al., 2004; Wyrick et al., 2004). Drainage of regolith into open fractures was proposed as a mechanism for the chains of pits on Phobos (Horstman and Melosh, 1989) and Mars (Wyrick et al., 2004). The results of analog models (Ferrill et al., 2004) supported the pit chain evolution proposed by Wyrick et al. (2004), suggesting that individual, isolated pits are the first features to form in the regolith as it begins to drain into the void created by dilation of a fracture at the surface (Fig. 8a). Model results showed that continued dilation at the surface caused individual pits to increase in diameter and ellipticity (Fig. 8b) prior to coalescing and forming partially merged pit chains (Fig. 8c). With continued dilation, pit chains further evolved (Fig. 8d) into fully merged pit chains with scalloped edges, where individual pits could no longer be resolved (Fig. 8e). Both modeled pits and those observed on Enceladus lack elevated rims and demonstrate a continuum of morphologies, ranging from isolated pits to evenly spaced pits of similar size, to scalloped linear depressions created by merged pits (Martin and Kattenhorn, 2013; Nahm and Kattenhorn, 2015). The strong morphological resemblance between analog models and the observed morphology of pit chains on Enceladus supports the interpretation that pit chains on Enceladus likely formed above dilated, extensional tectonic structures.

Regionally isolated linear and parallel sets of pit chains with distinct orientations on Enceladus are consistent with a spatially variable stress field (e.g., Patthoff and Kattenhorn, 2011); there is a variety of global and local stress mechanisms in which fractures may form parallel sets of fractures with regionally variable orientations (Collins et al., 2009). Furthermore, the parallel orientations of pit chains within individual sets suggest a common driving mechanism, stress field, and timing of formation. Extensional tectonics is a dominant process modifying the surfaces of the icy satellites of the outer solar system (Collins et al., 2009; Kattenhorn and Hurford, 2009). For example, pit chains on Phobos (frequently called grooves) (Horstman and Melosh, 1989) are likely the result of tidally induced extensional tectonics (Hurford et al., 2016), forming fracture sets similar to those observed on Enceladus. The observed morphology of individual pits and the continuum of pit chain morphologies on Enceladus, as well as the distribution of linear and parallel sets of pit chains on Enceladus, make extensional fracturing and/or dilational faulting our favored mechanism for pit chain formation on Enceladus.

### 3.2. Enceladus's regolith

The distribution of pit chains (Fig. 4) suggests that regolith is widely dispersed across Enceladus's surface, including in the cratered plains and across a small region of pit chains within the southern tectonized terrains near 60°E. Despite the limited presence of pit chains within Enceladus's tectonized terrains, the strong spatial correlation between cratered plains and pit chains raises two important points: (1) cratered plains must have an abundant mantle of loose regolith in which pit chains can form;

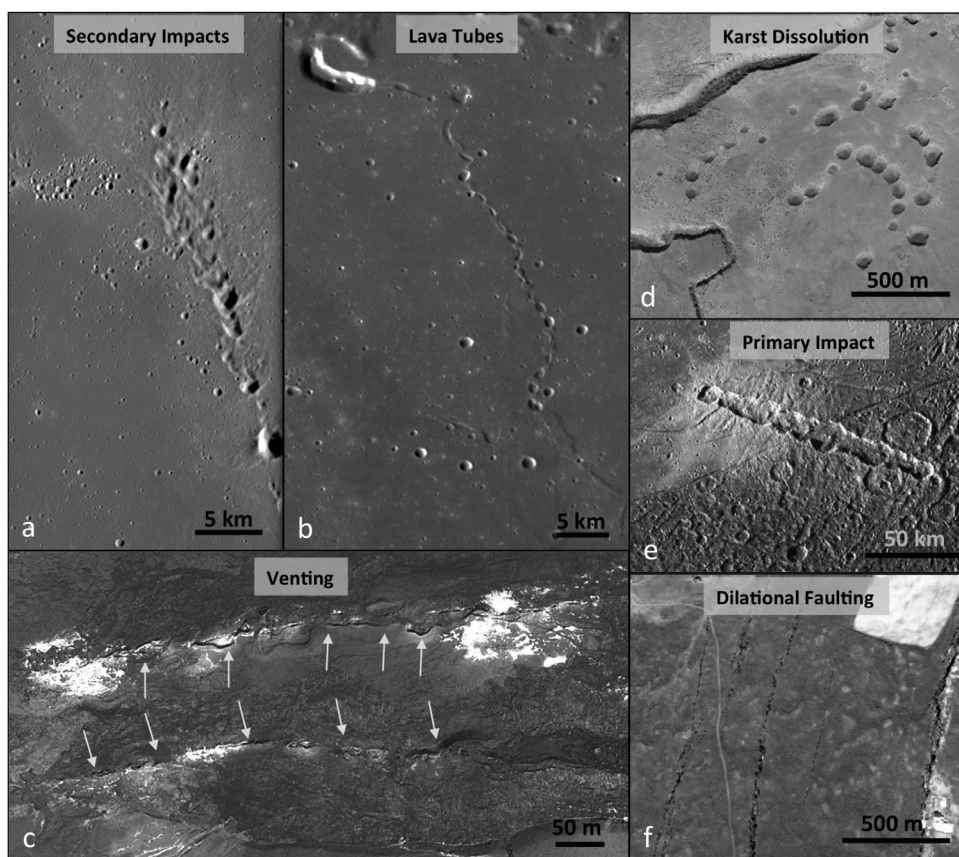


**Fig. 6.** Pit chains across the solar system with known or inferred formation mechanisms. **a.** Secondary impact chain on the Moon demonstrating a herringbone texture. Centered at 22.8796°N, 25.0183°W. Apollo image AS17-3093 (e.g. [McEwen and Bierhaus, 2006](#)). **b.** Lunar lava tube centered at 34°N, –43°E. From LRO WAC morphologic basemap mosaic. **c.** Linear chains of pits resulting from venting at Kilauea volcano in Hawaii. Image taken February 1, 2010 and obtained May 24, 2016 centered at 19.40177°N, 155.2758°W (from Google Earth). **d.** McCauly Sinks karst south of Winslow, AZ. Image taken October 12, 2012 and obtained May 24, 2016, centered at 34.7972°N, 110.5907°W (from Google Earth). **e.** Enki Catena primary crater chain on Ganymede. Image no. PIA01610. **f.** Pit chains resulting from dilational faulting in northwestern Iceland. Image taken July 27, 2012 and obtained May 24, 2016, centered at 66.0258°N, 165.840°W (from Google Earth) ([Ferrill et al., 2011](#)).

and (2) the cratered plains are in the process of being dissected by pit chains ([Fig. 5](#)), or were recently dissected (See [Section 2.3](#)). We do not suggest that the overall paucity of pit chains within the tectonized terrains necessarily signals the absence of regolith in these regions. Perhaps there is insufficient regolith across much of the tectonized terrains to create pit chains, or the pit chains are too nascent to be resolved with the current dataset. The lack of pit chains may also suggest that there is a fundamental rheological difference between the cratered plains and tectonized terrains that has allowed for the recent formation of pit chains in the cratered plains. While we suggest that the presence of pit chains on Enceladus is a way to detect regolith on the surface, we do not imply that the absence of pit chains is a proxy for the absence of regolith; it may be that the tectonic deformation that drives pit chain formation either has not occurred within the tectonized terrains, or has not been preserved.

A first-order estimate of the thickness of regolith can be inferred from the observed population of pit chains on Enceladus based on a geometric relationship of pit diameter and an assumed angle of repose. This method is similar to that used in studies of pit chains on Gaspra ([Veveřka et al., 1994](#)), Ida ([Sullivan et al., 1996](#)), and Eros ([Prockter et al., 2002](#)), which all use an angle of repose of 30° and the width of the pit chain measured perpendicular to strike to geometrically calculate regolith depth (assuming that pit depth is equal to regolith thickness). On Enceladus, pit diameters range from 300–1000 m, with a mean diameter of 583 m, which corresponds to a range of regolith depths of 90–290 m, or 168 m based on the mean pit diameter.

Regolith on Enceladus is likely to come from two potential sources: impacts and plume fall-back. Upper limits of impact-generated regolith (not including the mega-regolith of the upper crust) based on lunar highlands estimates are of the order of 8 m ([Bart et al., 2011](#)). We use the lunar values as a first order estimate of impact generated regolith on Enceladus, but acknowledge that 8 m likely reflects a minimum depth. The proposed impactor population for the Saturn system is, on average, two orders of magnitude greater than the lunar impactor population ([Dones et al., 2009](#)) with cratering rates at Enceladus estimated to be  $7.0 \times 10^{-14}$ – $5.7 \times 10^{-13}$  ([Zahnle et al., 2003](#)). A greater number of impactors in the Saturn system may suggest that Enceladus would experience a greater flux of impacts with respect to the Moon.

Modeled rates of plume-sourced regolith deposition on Enceladus vary with proximity to the jets ([Kempf et al., 2010](#)): the highest rate of 1 mm/yr is equivalent to 100 m/ $10^5$  years very near the jets. Near 45°S, modeled deposition is  $10^{-3}$  mm/yr ([Kempf et al., 2010](#)) or 100 m/ $10^8$  years. Around the equator, plume deposition is of the order of 100 m/ $10^9$  years. All estimated rates assume sustained plume activity through time and although these rates could deposit the estimated 90–290 m of regolith within the lifetime of Enceladus, so far there is insufficient evidence to determine the plume flux through time. Furthermore, the spatial distribution of plume fallout deposition rates shows a pattern that is broadly consistent with the observed pit chain distribution in that they both display similar (albeit slightly offset) antipodal distributions ([Kempf et al., 2010](#)). Discrepancies in the observed and modeled regolith distributions suggest that either the model needs refine-

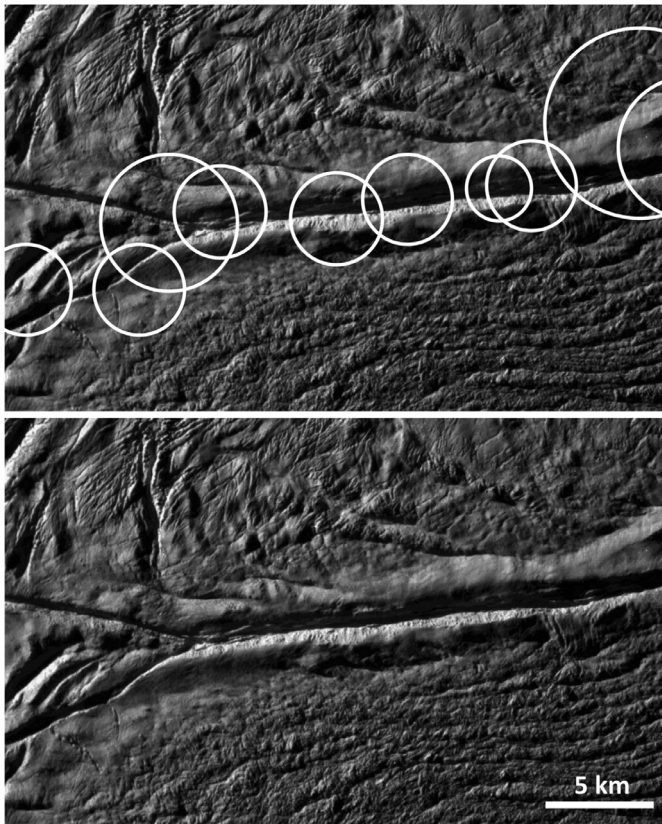


**Fig. 7.** Damascus Sulcus on Enceladus's South Polar Terrain. Image no. PIA11125, 33 m/pixel. Locations of jets 63–73 (left to right) from Porco et al. (2014); the circle diameter is the  $2\sigma$  uncertainty in jet location.

ment, that plumes have not been constant in rate or location over time, or that there are other methods for generating regolith that have yet to be considered. Ultimately, the observation of pit chains on Enceladus provides a way of detecting regolith distributed on

the surface, but cannot directly address how or when the regolith was emplaced.

### 3.3. Significance of regolith depth

Within regions of Enceladus where pit chains have been observed, the presence of a thick layer of regolith may have an insulating effect causing the top portion of the icy shell to be warmer (Passey and Shoemaker, 1982; Squyres et al., 1983; Passey, 1983; Bland et al., 2012). This phenomenon could mean that the effective surface temperature at the top of the brittle portion of the ice shell could be closer to 120 K (Bland et al., 2012; Passey and Shoemaker, 1982) instead of the observed 70 K at the surface (Spencer et al., 2006). These warmer temperatures would allow viscous relaxation to occur more easily, which has implications for understanding the relaxed state of craters observed across Enceladus and may help to refine parameters within thermal models (e.g., Bland et al., 2012; Mitri and Showman, 2008) giving better insight into the thermal evolution of Enceladus. Additionally, a layer of regolith would act to mute the morphology of the surface where such a layer occurs, in some ways mimicking the effects of topographic modification via viscous relaxation. Further work is needed to constrain the distribution of regolith depths across the surface of Enceladus, to better estimate the thermal state of the ice shell and the role regolith plays in modifying the surface morphology. However, to a first order, the distribution of pit chains presented here provides an indicator of the locations on Enceladus's surface where the presence of regolith could potentially have implications for the thermal state of the ice shell.

## 4. Conclusion

Detailed mapping of pit chains reveals a global distribution of these landforms that extends over a wide range of latitudes, from 60°S to 55°N, and across an almost global longitudinal range. Crosscutting relationships reveal pit chains to be some of the youngest features on the surface of Enceladus, suggesting that the

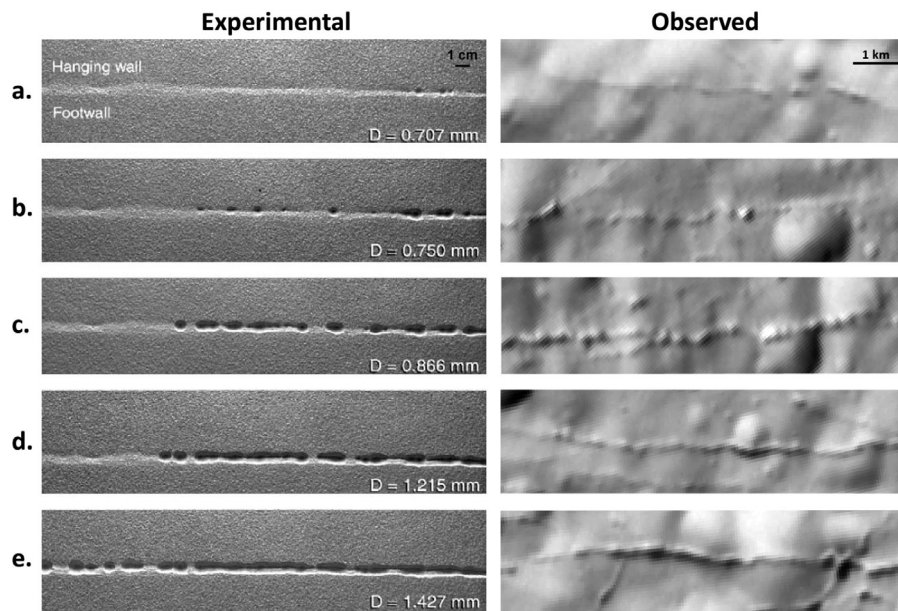


**Fig. 8.** Experimentally formed pit chains (left) (modified after Fig. 4 in Ferrill et al., 2004) formed above a high angle normal fault ( $D$  is the amount of dilation in the experimental set-up), compared with pit chains on the cratered plains of Enceladus (right). As dilation proceeds in the Ferrill et al. (2004) analog work, isolated pits (a, b.) form with a regular spacing (c), and finally merge together (d) into a continuous scalloped trough (e). All of these morphological stages are also observed in the cratered plains of Enceladus, for which we infer a similar evolutionary sequence. (Observed images centered at: a. 5.714°S, 156.672°E b. 10.285°S, 163.285°E, c. 8.128°S, 163.119°E, d. 3.15°S, 158.11°E, e. 7.911°S, 158.239°E).

cratered terrains have recently undergone extensional tectonic deformation. Pit chains form in assemblages of parallel sets with distinct orientations, preserving of a history of tectonic deformation of the cratered terrains. A number of mechanisms have been proposed to account for pit chain formation across the solar system. The morphology and distribution of pit chains on Enceladus, however, are consistent with formation in association with extension fractures or dilational faulting. This mechanism, in particular, requires that a thick layer of loose regolith be present on the surface, in which pits form as regolith drains into a subsurface fracture. Estimates of regolith depth range from 90–290 m deep, based on the diameter of individual pits. Enceladus's regolith is likely generated from impact cratering and fall-back from Enceladus's plume. Understanding the distribution of regolith on Enceladus's surface is important, as it may provide an insulating effect at the surface, influencing the effective surface temperature and the thermal state of Enceladus's icy shell.

## Acknowledgements

This work was supported by NASA OPR Grant #NNX08AQ94 and NSSF Grant #NNX11AP30H. The portion of this work performed by RTP was carried out at the Jet Propulsion Laboratory, California Institute of Technology, under a contract with the National Aeronautics and Space Administration. This research has made use of the USGS Integrated Software for Imagers and Spectrometers (ISIS). The Authors would also like to acknowledge Amanda L. Nahm and Paul K. Byrne for their helpful reviews of the original manuscript.

## References

- Bart, G.D., Nickerson, R.D., Lawder, M.T., Melosh, H.J., 2011. Global survey of lunar regolith depths from LROC images. *Icarus* 215, 485–490. doi:10.1016/j.icarus.2011.07.017.
- Bland, M.T., Singer, K.N., McKinnon, W.B., Schenk, P.M., 2012. Enceladus' extreme heat flux as revealed by its relaxed craters. *Geophys. Res. Lett.* 39, L17204. doi:10.1029/2012GL052736.
- Bleamaster, Leslie, F.III, Hansen, V.L., 2004. Effects of crustal heterogeneity on the morphology of Chasmata, Venus. *J. Geophys. Res.* 109, E02004. doi:10.1029/2003JE002193.
- Bray, V.J., Smith, D.E., Turtle, E.P., Perry, J.E., Rathbun, J.A., Barnash, A.N., Helfenstein, P., Porco, C.C., 2007. Impact crater morphology variations on Enceladus. Paper Presented at the 38th Lunar and Planetary Science Conference Abstract #1873.
- Brown, R.H., Clar, R.N., Buratti, B.J., Cruikshank, D.P., Barnes, J.W., Mastrapa, R.M.E., Bauer, J., Newman, S., Momary, T., Baines, K.H., Bellucci, G., Capaccioni, F., Ceroni, P., Combes, M., coradini, A., Drossart, P., Formisano, V., Jaumann, R., Langevin, Y., Matson, D.L., McCord, T.B., Nelson, R.M., Nicholson, P.D., Sicardy, B., Sotin, C., 2006. Composition and physical properties of Enceladus' surface. *Science* 311, 1425. doi:10.1126/science.1125018.
- Buczkowski, D.L., Barnouin-Jha, O.S., Prockter, L.M., 2008. 433 Eros lineaments: global mapping and analysis. *Icarus* 193, 39–52. doi:10.1016/j.icarus.2007.06.028.
- Buczkowski, D.L., Wyrick, D.Y., Iyer, K.A., Kahn, E.G., Scully, J.E.C., Nathues, A., Gaskell, R.W., Roatsch, T., Preusker, F., Schenk, P.M., Le Corre, L., Reddy, V., Yingst, R.A., Mest, S., Williams, D.A., Garry, W.B., Barnouin, O.S., Jaumann, R., Raymond, C.A., Russell, C.T., 2012 a. Large-scale troughs on Vesta: a signature of planetary tectonics. *Geophys. Res. Lett.* 39, L18205. doi:10.1029/2012GL052959.
- Buczkowski, D.L., Wyrick, D.Y., Capaccioni, F., Scully, J.E.C., Williams, D.A., Hiesinger, H., Garry, W.B., Yingst, R.A., Le Corre, L., Nathues, A., Schenk, P.M., Jaumann, R., Raymond, C.A., Pieters, C.M., Roatsch, T., Preusker, F., Russell, C.T., 2012 b. Geologic mapping of the AV-9 Numisia quadrangle of asteroid 4Vesta. 43rd Lunar and Planetary Science Conference Abstract # 2263.
- Buczkowski, D.L., DeSanctis, M.C., Raymond, C.A., Wyrick, D.Y., Ammannito, E., Frigeri, A., Williams, D., Russell, C.T., 2013. Brumalia Tholus: an indication of magmatic intrusion on Vesta. 44th Lunar and Planetary Science Conference Abstract #1996.
- Collins, G.C., McKinnon, W.B., Moore, J.M., Nimmo, F., Pappalardo, R.T., Prockter, L.M., Schenk, P.M., 2009. In: Watters, T.R., Schultz, R.A. (Eds.), *Tectonics of the Outer Planet Satellites in Planetary Tectonics*. Cambridge University Press.
- Crow-Willard, E.N., Pappalardo, R.T., 2015. Structural mapping of Enceladus and implications for formation of tectonized regions. *Icarus* 120, doi:10.1002/2015/JE004818.
- Cruikshank, K.M., Aydin, A., 1995. Unweaving the joints in Entrada sandstone, Arches National Park, Utah, U.S.A. *J. Struct. Geol.* 17, 409–421.
- Cushing, G.E., Titus, T.N., Wynne, J.J., Christensen, P.R., 2007. THEMIS observes possible cave skylights on Mars. *Geophys. Res. Lett.* 34, L17201. doi:10.1029/2007GL030709.
- Dones, L., Chapman, C.R., McKinnon, W.B., Melosh, H.J., Kirchoff, M.R., Neukum, G., Zahnle, K., 2009. Icy satellites of Saturn: impact cratering and age determination. In: Dougherty, M.K., Esposito, L., Krimigis, S. (Eds.), *Saturn from Cassini-Huygens*. Springer, pp. 613–616.
- Ferrill, D.A., Morris, A.P., Wyrick, D.Y., Sims, D.W., Franklin, N.M., 2004. Dilational fault slip and pit chain formation on Mars. *GSA Today* 14 (10), 4–12. doi:10.1130/1052-5173(2004)014(4:DFSAPC)2.0.CO;2.
- Ferrill, D.A., Wyrick, D.Y., Smart, K.J., 2011. Coseismic, dilational-fault and extension-fracture related pit chain formation in Iceland: analog for pit chains on Mars. *Lithosphere* 3 (2), 133–142. doi:10.1130/L123.1.
- Haruyama, J., Kioki, K., Shirao, M., Morota, T., Hiesinger, H., van der Bogert, C.H., Miyamoto, H., Iwasaki, A., Yokota, Y., Ohtake, M., Matsunaga, T., Hara, S., Nakanotani, S., Pieters, C.M., 2009. Possible lunar lava tube skylight observed by SE-LENE cameras. *Geophys. Res. Lett.* 36, L21206. doi:10.1029/2009GL040635.
- Horstman, K.C., Melosh, H.J., 1989. Drainage pits in cohesionless materials: implications for the surface of Phobos. *J. Geophys. Res.* 94 (12) 433–12,441. doi:10.1029/JB094iB09p12433.
- Hurford, T.A., Asphaug, E., Spitale, J.N., Hemingway, D., Rhoden, A.R., Henning, W.G., Bills, B.G., Kattenhorn, S.A., Walker, M., 2016. Tidal disruption of Phobos as the cause of surface fractures. *J. Geophys. Res.* 121, 1054–1065. doi:10.1002/2015JE004943.
- Kattenhorn, S.A., Hurford, T., 2009. Tectonics of Europa. In: Pappalardo, R.T., McKinnon, W.B., Khurana, K. (Eds.), *Europa*. The University of Arizona Press.
- Kargel, J.S., 1984. A crater chain on Enceladus: evidence for explosive water volcanism. In: 15th Lunar and Planetary Science Conferences, pp. 427–428.
- Kempf, S., Beckmann, U., Schmidt, J., 2010. How the Enceladus dust plume feeds Saturn's E ring. *Icarus* 206, 446–457. doi:10.1016/j.icarus.2009.09.016.
- Kieffer, S.W., Lu, X., Bethke, C.M., Spencer, J.R., Marshak, S., Navrotsky, A., 2006. A clathrate reservoir hypothesis for Enceladus' south polar plume. *Science* 314, 1764. doi:10.1126/science.1133519.
- Kirchoff, M.R., Schenk, P., 2009. Crater modification and geologic activity in Enceladus' heavily cratered plains: evidence from the impact crater distribution. *Icarus* 202, 656–668. doi:10.1016/j.icarus.2009.03.034.
- Kite, E.S., Rubin, A.M., 2016. Sustained eruptions on Enceladus explained by turbulent dissipation in tiger stripes. *PNAS* 113, 3971–3975. doi:10.1073/pnas.1520507113.
- Martin, E.S., Kattenhorn, S.A., 2013. Probing regolith depths on Enceladus by exploring a pit chain proxy. 44th Lunar and Planetary Science Conference Abstract #2047.
- Martin, E.S., Kattenhorn, S.A., 2014. A history of pit chain formation within Enceladus' cratered terrains suggests a nonsynchronous rotation stress field. 45th Lunar and Planetary Science Conferences Abstract #1083.
- Martin, E.S., 2016. The distribution and characterization of strike-slip faults on Enceladus. *Geophys. Res. Lett.* 43, 2456–2464. doi:10.1002/2016GL067805.
- McEwen, A.S., Bierhaus, E.B., 2006. The importance of secondary cratering to age constraints on planetary surfaces. *Annu. Rev. Earth Planet. Sci.* 34, 535–567. doi:10.1146/annurev.earth.34.031405.125018.
- Michaud, R.L., Pappalardo, R.T., Collins, G.C., 2008. Pit chains on Enceladus: a discussion of their origin. 39th Lunar and Planetary Science Conference Abstract #1678.
- Mitri, G., Showman, A.P., 2008. Thermal convection in ice-I shells of Titan and Enceladus. *Icarus* 193, 387–396. doi:10.1016/j.icarus.2007.07.016.
- Nahm, A.L., Kattenhorn, S.A., 2015. A unified nomenclature for tectonic structures on the surface of Enceladus. *Icarus* 258, 67–81.
- Nimmo, F., Spencer, J.R., Pappalardo, R.T., Mullen, M.E., 2007. Shear heating as the origin of the plumes and heat flux on Enceladus. *Nature* 447, 289–291. doi:10.1038/nature05783.
- Oberbeck, V.R., Morrison, R.H., 1974. Laboratory simulation of the herringbone pattern associated with lunar secondary crater chains. *The Moon* 9, 415–455.
- Okubo, C.H., Martel, S.T., 1998. Pit crater formation on Kilauea volcano, Hawaii. *J. Volcanol. Geotherm. Res.* 86, 1–18. doi:10.1016/S0377-0273(98)00070-5.
- Passey, Q.R., 1983. Viscosity of the lithosphere of Enceladus. *Icarus* 53, 105–120. doi:10.1016/0019-1035(83)90024-6.
- Passey, Q.R., Shoemaker, E.M., 1982. Craters and basins on Ganymede and Callisto: morphological indicators of crustal evolution. In: Morrison, D. (Ed.), *Satellites of Jupiter*. Univ. of Ariz. Press, Tucson, pp. 379–434.
- Patthoff, D.A., Kattenhorn, S.A., 2011. A fracture history on Enceladus provides evidence for a global ocean. *Geophys. Res. Lett.* 38, L18201. doi:10.1029/2011GL048387.
- Patthoff, D.A., Pappalardo, R.T., Chilton, H., Thomas, P., 2014. Enceladus's diverse ridged terrains. *Geol. Soc. Am. Abstr. Programs* 46 (6), 219 Paper #84-10.
- Pike, R.J., Wilhelms, D.E., 1978. Secondary-impact craters on the Moon: topographic form and geologic process. In: 9th Lunar and Planetary Science Conference, Abstract, pp. 907–909.
- Porco, C.C., Helfenstein, P., Thomas, P.C., Ingersoll, A.P., Wisdom, J., West, R., Neukum, G., Denk, T., Wagner, R., Roatsch, T., Kieffer, S., Turtle, E., McEwen, A., Johnson, T.V., Rathbun, J., Veverka, J., Wilson, D., Perry, J., Spitale, J., Brahic, A., Burns, J.A., DelGenio, A.D., Dones, L., Murray, C.D., Squyres, S., 2006. Cassini observes the active south pole of Enceladus. *Science* 311, 1393–1401. doi:10.1126/science.1123013.
- Porco, C.C., DiNino, D., Nimmo, F., 2014. How the geysers, tidal stresses, and thermal emission across the south polar terrain of Enceladus are related. *ApJ* 148:45. doi:10.1088/0004-6256/148/3/45.
- Prockter, L., Thomas, P., Robinson, M., Joseph, J., Milne, A., Bussey, B., Veverka, J., Cheng, A., 2002. Surface expressions of structural features on Eros. *Icarus* 155, 75–93. doi:10.1006/icar.2001.6770.

- Roatsch, Th., Kersten, E., Hoffmeister, A., Wählich, M., Matz, K.-D., Porco, C.C., 2013. Recent improvements of the Saturnian satellites atlases: Mimas, Enceladus, and Dione. *Planet. Space Sci.* 77, 118–125. doi:[10.1016/j.pss.2012.02.016](https://doi.org/10.1016/j.pss.2012.02.016).
- Schenk, P.M., McKinnon, W.B., 2009. One-hundred-km-scale basins on Enceladus: evidence for an active ice shell. *Geophys. Res. Lett.* 36, L16202. doi:[10.1029/2009GL039916](https://doi.org/10.1029/2009GL039916).
- Spencer, J.R., Pearl, J.C., Segura, M., Flasar, F.M., Mamoutkine, A., Romani, P., Bu-ratti, B.J., Hendrix, A.R., Spilker, L.J., Lopes, R.M.C., 2006. Cassini encounters Enceladus: background and the discovery of a south polar hot spot. *Science* 311 (5766), 1401–1405. doi:[10.1126/science.1121661](https://doi.org/10.1126/science.1121661).
- Spencer, J.R., Barr, A.C., Esposito, L.W., Helfenstein, P., Ingersoll, A.P., Jaumann, R., McKay, C.P., Nimmo, F., Waite, J.H., 2009. *Enceladus: An Active Cryovolcanic Satellite in Saturn from Cassini-Huygens*. Springer, Dordrecht, pp. 683–724.
- Spitale, J.N., Hurford, T.A., Rhoden, A.R., Berkson, E.E., Platts, S.S., 2015. Curtain eruptions from Enceladus' south-polar terrain. *Nature* 521, 57–60. doi:[10.1038/nature14368](https://doi.org/10.1038/nature14368).
- Squyres, S.W., Reynolds, R.T., Cassen, P.M., 1983. The Evolution of Enceladus. *Icarus* 53, 319–331. doi:[10.1016/0019-1035\(83\)90152-5](https://doi.org/10.1016/0019-1035(83)90152-5).
- Sullivan, R., Greeley, R., Pappalardo, R., Asphaug, E., Moore, J.M., Morrison, D., Bel-ton, M.J.S., Carr, M., Chapman, C.R., Geissler, P., Greenberg, R., Granahan, J., Head, J.W.III, Kirk, R., McEwen, A., Lee, P., Thomas, P.C., Veverka, J., 1996. Ge-ology of 243 Ida. *Icarus* 120, 119–139. doi:[10.1006/icar.1996.0041](https://doi.org/10.1006/icar.1996.0041).
- Thomas, P., Veverka, J., Bloom, A., Duxbury, T., 1979. ), Grooves on Phobos: their distribution, morphology and possible origin. *J. Geophys. Res.* 84, 8457–8477. doi:[10.1029/JB084iB14p08457](https://doi.org/10.1029/JB084iB14p08457).
- Thordarson, T., Larsen, G., 2007. Volcanism in Iceland in historical time: volcano types, eruption styles and eruptive history. *J. Geodyn.* 43, 118–153. doi:[10.1016/j.jog.2006.09.005](https://doi.org/10.1016/j.jog.2006.09.005).
- Veverka, J., Thomas, P., Simonelli, D., Belton, M.J.S., Carr, M., Chapman, C., Davies, M.E., Greeley, R., Greenberg, R., Head, J., Klaasen, K., Johnson, T.V., Morri-son, D., Neukum, G., 1994. Discovery of grooves on Gaspra. *Icarus* 107, 399–411. doi:[10.1006/icar.1994.1007](https://doi.org/10.1006/icar.1994.1007).
- Wyrrick, D., Ferrill, D.A., Morris, A.P., Colton, S.L., Sims, D.W., 2004. Distribution, mor-phology, and origins of Martian pit crater chains. *J. Geophys. Res.* 109, E06005. doi:[10.1029/2004JE002240](https://doi.org/10.1029/2004JE002240).
- Wyrrick, D.Y., Buczkowski, D.L., Bleamaster, L.F., Collins, G.C., 2010. Pit crater chains across the solar system. *41st Lunar and Planetary Science Conference Abstract*, #1413.
- Zahnle, K., Schenk, P., Levison, H., Dones, L., 2003. Cratering rates in the outer solar system. *Icarus* 163, 263–289. doi:[10.1016/S0019-1035\(03\)00048-4](https://doi.org/10.1016/S0019-1035(03)00048-4).